

## PARTICLE CANDIDATES FOR DARK MATTER: A CASE FOR (DOMINANT OR SUBDOMINANT) RELIC NEUTRALINOS

A. Bottino, N. Fornengo, S. Scopel

*Dipartimento di Fisica Teorica, Università di Torino  
and INFN, Sez. di Torino, Via Giuria 1, I-10125 Torino, Italy*

F. Donato

*Laboratoire de Physique Théorique LAPTH, B.P. 110, F-74941*

*Annecy-le-Vieux Cedex, France*

*and INFN, Sede di Presidenza, 00186 Roma, Italy*

### Abstract

After a short introduction on particle candidates for dark matter within possible extensions of the standard model, we concentrate on Weakly Interacting Massive Particles, and on one of their most interesting physical realizations: the neutralino. We analyze how detectability of relic neutralinos by direct and indirect means is related to their local and cosmological densities; we use simple general arguments to discuss different scenarios where relic neutralinos make up the dominant bulk of dark matter or only a small fraction of it. Our general arguments are further corroborated by specific numerical results. We show to which extent the present experiments of direct searches for WIMPs, when interpreted in terms of relic neutralinos, probe interesting regions of the supersymmetric parameter space. Our analysis is performed in a number of different supersymmetric schemes.

## 1 Introduction

Evidence for existence of dark matter and dark energy in the Universe is provided by a host of observational data: properties of galactic halos and clusters of galaxies, large scale structures, cosmic microwave background, high-redshift supernovae SNe Ia. As far as dark matter is concerned, a favorite range for  $\Omega_m h^2$  ( $\Omega_m$  being the matter density divided by the critical density and  $h$  the present-day value of the Hubble constant in units of  $\text{km} \cdot \text{s}^{-1} \cdot \text{Mpc}^{-1}$ ) may be set as:  $0.05 \lesssim \Omega_m h^2 \lesssim 0.3$ . Notice that the most recent determinations of cosmological parameters <sup>1)</sup> appear to pin down the matter relic abundance to a narrower range  $0.08 \lesssim \Omega_m h^2 \lesssim 0.21$ ; however, some caution in taking this range too rigidly is advisable, since some determinations of cosmological parameters are still subject to fluctuations. We point out that in the present paper we do not restrict ourselves to any particular interval of  $\Omega_m h^2$ ; only some features of Figs. 7-8, depend on the actual value employed for the minimum amount of matter necessary to reproduce the halo properties.

## 2 Particle candidates for dark matter

Various possible extensions of the standard model, envisaged in particle physics for reasons quite independent of any cosmological motivation, offer, as an extra bonus, a great variety of particle candidates for dark matter.

A very natural candidate is the neutrino: both a light neutrino, with a mass  $m_\nu \lesssim 1$  eV, or a heavy one, with a mass  $m_\nu \gtrsim 100$  GeV, might be viable and interesting candidates. The light neutrino will be briefly discussed in the next section.

What appears to be the most natural (though certainly not the unique) solution of the strong CP-violation, the axion <sup>2)</sup>, would also be an appealing candidate for dark matter; in fact, though already constrained by a number of observational data, the axion still offers interesting cosmological perspectives. Lack of space does not allow here a presentation of the current situation; we refer to Ref. <sup>3)</sup> for an overview of this subject.

One of the most favorite candidates for dark matter is the neutralino, which in many supersymmetric schemes turns out to be the Lightest Supersymmetric Particle (LSP). Supersymmetry is known to be motivated by a number of strong theoretical arguments, though it is not yet supported by experimental evidence, except for a few possible hints: unification of coupling constants at the grand unification scale <sup>4)</sup>, Higgs LEP events <sup>5, 6, 7)</sup>, muon anomalous magnetic mo-

ment 8, 9, 10, 14) (the two latter points will be briefly discussed in Sect. 5). If supersymmetry exists in Nature and the R-parity is conserved, the LSP would be stable. Depending on the susy-breaking mechanism and on the sectors of the susy parameter space, the LSP may be one of many options: sleptons, squarks, gluino, gravitino, neutralino, axino (if the axion exists). When weakly interacting, the LSP has the prerequisites for being a good dark matter candidate. In the present note we discuss in detail the neutralino, whose detection rates may reach the level of current experimental sensitivities, both as a dominant or a subdominant component of dark matter. Other possible susy candidates are not discussed here.

### 3 Decoupling of particles from the primordial plasma

In the standard scenario of the early Universe, relic particles originate from their decoupling from the primordial plasma, while in thermic equilibrium; the decoupling of any single species occurred when the interaction rate of that species with the thermic plasma became smaller than the expansion rate of the Universe (at the so-called freeze-out temperature). It is customary to define as hot (cold) candidates those particles that are relativistic (non relativistic), when they decoupled from the thermal medium.

A typical case of hot candidates is provided by neutrinos with a small mass,  $m_\nu \lesssim 1$  MeV. Their present-day relic abundance turns out to be  $\Omega_\nu h^2 = \sum_\nu m_\nu / (93 \text{ eV})$ . Actually, we already have some indications of non-vanishing neutrino masses. The present experimental data may be formulated in terms of difference in squared masses, namely:  $\Delta m^2 \sim 10^{-5} - 10^{-4} \text{ eV}^2$  from solar neutrinos (if MSW effect is at work) <sup>15)</sup>,  $\Delta m^2 \sim (2 - 5) \times 10^{-3} \text{ eV}^2$  from atmospheric neutrinos <sup>16)</sup>,  $0.2 \text{ eV}^2 \lesssim \Delta m^2 \lesssim 1 \text{ eV}^2$  from the LSND experiment <sup>17)</sup>.

Using the data on atmospheric neutrinos, a conservative estimate gives:  $\Omega_\nu h^2 \gtrsim 5 \times 10^{-4}$ , *i.e.* a value of relic abundance which, although small, is already at the level of the average density of visible matter. Notice that  $\Omega_\nu h^2$  could be sizeably larger, in case of a degeneracy in neutrino masses. Unfortunately, at present, no experimental device is capable of measuring these low-energy neutrinos ( $T_\nu = 1.95 \text{ K}$ ). Finally, we recall that light neutrinos cannot comprise the whole bulk of dark matter; indeed, should they constitute a dominant dark matter component, one would have difficulties in generating the present cosmological structures.

A generic Weakly Interacting Massive Particle (WIMP) would behave as a cold dark matter candidate. Its relic abundance may be derived to be

$$\Omega_{WIMP} h^2 \sim \frac{10^{-37} \text{cm}^2}{\langle \sigma_{ann} v \rangle}, \quad (1)$$

where  $\sigma_{ann}$  and  $v$  are the WIMP pair-annihilation and the relative velocity, respectively.  $\langle \sigma_{ann} v \rangle$  denotes the thermal average of the product  $(\sigma_{ann} \cdot v)$  integrated from the freeze-out temperature to the present-day one. What is remarkable is that for a number of particle candidates it is conceivable that  $\Omega_{WIMP} h^2$ , as given in Eq. (1), may be of order 0.1 – 1. Even more noticeable is the fact that for some candidates with  $\Omega_{WIMP} h^2 = \text{O}(0.1)$  the detection rates are at the level of current experimental sensitivities. This is the case of the neutralino, which will be discussed at some length in the following. However, it is obvious that detectability of any given candidate is of the utmost importance, also in the case of a relic particle which can only contribute for a fraction of the total dark matter density. We will examine this point in Sect. 4.3.

One should be aware that also decoupling mechanisms different from the standard one are viable. An interesting example is provided by the low reheating-temperature scenario, discussed in Ref. 18). For instance, in this case the WIMP relic abundance could be proportional to  $\sigma_{ann}$ , at variance with Eq. (1). Thus, the relevant WIMP phenomenology could be quite different from the one depicted in the rest of this note.

Dark matter particles may also be produced non-thermally (see, for instance, Ref. 19) for a review and Ref. 20) for a specific realization leading to relic neutralinos).

## 4 Direct and indirect signals of WIMPs

Different strategies for detecting the presence of WIMPs in our halo have been envisaged. The present note is mostly devoted to an analysis of the discovery potential of the direct searches for WIMPs, though some considerations on the indirect means are also included.

### 4.1 WIMP direct detection

The most natural experimental mean for detecting WIMPs is based on the measurement of the recoil that a nucleus of an appropriate detector would suffer, when hit by a WIMP. Various methods may be employed for the detection of the recoil energy 21). With the present experimental sensitivities, the only signature for disentangling the signal from the background is based on the annual-modulation effect

of the signal, due to the composition of the solar-system speed relative to the dark halo with the rotational velocity of the Earth around the Sun<sup>22)</sup>. As we show in the following, the discovery potential of WIMP direct searches confers to this experimental mean a prominent role in the investigation of particle dark matter.

Experiments for WIMP direct detection provide a measurement (or an upper bound) of the differential event rate

$$\frac{dR}{dE_R} = N_T \frac{\rho_W}{m_W} \int d\vec{v} f(\vec{v}) v \frac{d\sigma}{dE_R}(v, E_R), \quad (2)$$

where  $N_T$  is the number of the target nuclei per unit of mass,  $m_W$  is the WIMP mass,  $\rho_W$  is the local WIMP matter density,  $\vec{v}$  and  $f(\vec{v})$  denote the WIMP velocity and the velocity distribution function in the Earth frame ( $v = |\vec{v}|$ ) and  $d\sigma/dE_R$  is the WIMP–nucleus differential cross section. The nuclear recoil energy,  $E_R$ , is given by  $E_R = m_{\text{red}}^2 v^2 (1 - \cos\theta^*)/m_N$ , where  $\theta^*$  is the scattering angle in the WIMP–nucleus center–of–mass frame,  $m_N$  is the nuclear mass and  $m_{\text{red}}$  is the WIMP–nucleus reduced mass. Eq.(2) refers to the case of a monoatomic detector, like the Ge detectors. Its generalization to more general situations, like for instance the case of NaI, is straightforward. In what follows,  $\rho_W$  will be factorized in terms of the local value for the total non–baryonic dark matter density  $\rho_l$  and of the fractional amount of density,  $\xi$ , contributed by the candidate WIMP, *i.e.*  $\rho_W = \xi \cdot \rho_l$ . For  $\rho_l$  we use the range  $0.2 \text{ GeV cm}^{-3} \leq \rho_l \leq 0.7 \text{ GeV cm}^{-3}$ , where the upper side of the range takes into account the possibility that the matter density distribution is not spherical, but is described by an oblate spheroidal distribution<sup>23, 24)</sup>.

The WIMP–nucleus differential cross section may conveniently be split into a coherent part and a spin–dependent one  $\frac{d\sigma}{dE_R} = \left(\frac{d\sigma}{dE_R}\right)_C + \left(\frac{d\sigma}{dE_R}\right)_{SD}$ , whose generic features are discussed in the seminal paper of Ref.<sup>25)</sup>. To compare theoretical expectations with experimental data, and experimental data of different detectors among themselves, it is useful to convert the WIMP–nucleus cross–section into a WIMP–nucleon cross section. Under the hypothesis that the coherent cross–section is dominant and the WIMP couples equally to protons and neutrons (at least approximately), the WIMP–nucleus cross section may be expressed in terms of a WIMP–nucleon scalar cross section  $\sigma_{\text{scalar}}^{(\text{nucleon})}$  as<sup>26)</sup>

$$\frac{d\sigma}{dE_R} \simeq \left(\frac{d\sigma}{dE_R}\right)_C \simeq \frac{F^2(q)}{E_R^{\text{max}}} \left(\frac{1 + m_W/m_p}{1 + m_W/m_N}\right)^2 A^2 \sigma_{\text{scalar}}^{(\text{nucleon})}, \quad (3)$$

where  $m_p$  is the proton mass,  $A$  is the nuclear mass number,  $E_R^{\text{max}}$  is the maximal recoil energy and  $F(q)$  is the nuclear form factor for coherent interactions, usually

parametrized in the Helm form <sup>27)</sup>. In the following we assume that the previous conditions are satisfied, so that, by using Eq. (3), a WIMP–nucleon scalar cross section  $\sigma_{\text{scalar}}^{(\text{nucleon})}$  may be derived from the WIMP–nucleus cross section.

From the general formula in Eq. (2), it is clear that, in order to extract a WIMP–nucleus cross section from the experimental data, one has to use a specific expression for the velocity distribution function  $f(\vec{v})$  (in writing Eq. (2) we have already assumed that the WIMP phase–space distribution function is factorizable as  $\rho(\vec{r}) \cdot f(\vec{v})$ , though this is certainly not the most general case <sup>23)</sup>). The usual choice for  $f(\vec{v})$  is the isotropic Maxwell–Boltzmann distribution in the galactic rest frame, as derived from the isothermal–sphere model. The results from WIMP direct measurements, as derived by employing the standard isotropic Maxwell–Boltzmann distribution, will be presented in the following section; the consequences of using other WIMP distributions will be discussed in Sect. 4.1.2.

#### 4.1.1 Results from WIMP direct measurements

In Fig. 1 we summarize the most recent experimental results of WIMP direct measurements <sup>28, 29, 30, 31, 32, 33, 34, 35)</sup> in terms of  $\sigma_{\text{scalar}}^{(\text{nucleon})}$  as a function of the WIMP mass. In deriving the plots of Fig. 1, the isotropic Maxwell–Boltzmann distribution has been used for the velocity distribution  $f(\vec{v})$  and the local WIMP density has been set at the *default* value  $\rho_l = 0.3 \text{ GeV cm}^{-3}$ . The open curves denote upper bounds, the closed one denotes the 3– $\sigma$  region, derived from the annual–modulation effect measured by the DAMA Collaboration <sup>33, 34)</sup>.

It has been shown <sup>36, 37, 38, 39, 40, 41)</sup> that the DAMA annual–modulation effect may be interpreted as due to relic neutralinos, whose relic abundance may also be in the range of cosmological interest. Comparisons of the experimental data of Ref. <sup>34)</sup> with susy calculations have also been presented in Refs. <sup>42, 43, 44, 45, 46)</sup>. In Sect. 5 we will discuss these properties, by proving that the current direct experiments for WIMPs, when interpreted in terms of relic neutralinos, probe regions of the supersymmetric parameter space compatible with all present bounds from accelerators.

#### 4.1.2 Dependence on the WIMP distribution function in the halo

Let us now discuss some properties related to the use of WIMP distribution functions different from the standard Maxwell–Boltzmann distribution. Recent investigations have shown that deviations from this standard scheme, either due to a bulk rotation of the dark halo <sup>47, 48)</sup> or to an asymmetry in the WIMP velocity distribution

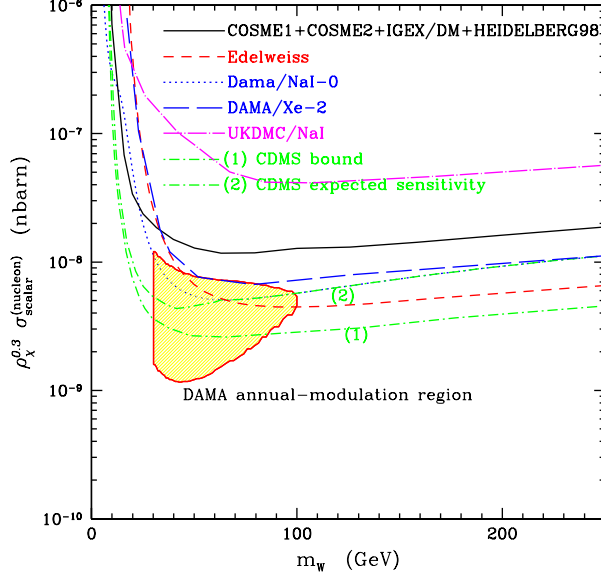


Figure 1: *Experimental results of WIMP direct measurements* <sup>28–35)</sup> *in terms of*  $\xi \sigma_{\text{scalar}}^{(\text{nucleon})}$  *as a function of the WIMP mass*  $m_W$ . *The isotropic Maxwell–Boltzmann distribution has been used for the velocity distribution*  $f(\vec{v})$  *and the local WIMP density has been set at the default value*  $\rho_l = 0.3 \text{ GeV cm}^{-3}$ . *The open curves denote upper bounds, the closed one denotes the 3- $\sigma$  region, derived from the annual-modulation effect measured by the DAMA Collaboration* <sup>33, 34)</sup>.

49, 50, 51), influence the determination of the WIMP–nucleus cross sections from the experimental data in a sizeable way. In Ref. <sup>50)</sup> also triaxial matter distributions are considered; in the present paper deviation from sphericity in the WIMP matter distributions are taken into account only through the physical range allowed for the value of  $\rho_l$  (see our previous comment on  $\rho_W$  after Eq. (2)). In the typical plots of  $\sigma_{\text{scalar}}^{(\text{nucleon})}$  vs  $m_W$ , as the ones displayed in Fig. 1, the effect introduced by the mentioned deviations from the Maxwell–Boltzmann is generically to elongate the contours towards larger values of  $m_W$ . This is for instance the case for the the annual–modulation region of the DAMA Collaboration <sup>34)</sup>. In Fig. 3 of Ref. <sup>38)</sup> it is shown that, by implementing the dark halo with a bulk rotation according to the treatment in Ref. <sup>48)</sup>, the annual–modulation region moves towards larger values of the WIMP mass, with an elongation which brings the right–hand extreme from the value of  $\sim 150 \text{ GeV}$  to  $\sim 200 \text{ GeV}$ . A similar effect is obtained by introducing an asymmetry in the WIMP velocity distribution  $f(\vec{v})$ : Fig. 4 of Ref. <sup>51)</sup> illustrates this point; notice that this asymmetry effect also pushes somewhat downwards the

annual-modulation region. We emphasize that all these effects are extremely important, when experimental results of WIMP direct detection are being compared with theoretical models for specific candidates. This point has been overlooked in most analyses in terms of relic neutralinos.

#### 4.1.3 WIMP local density

The values to be assigned to the WIMP local density  $\rho_W = \xi \cdot \rho_l$  have to be consistent with the values of the WIMP relic abundance, as derived from evaluations for any given specific WIMP candidate. For the case considered in detail in the following, the neutralino, we proceed in the following way. The relic abundance  $\Omega_\chi h^2$  is evaluated in specific supersymmetric schemes (see Sect. V). When  $\Omega_\chi h^2 \geq (\Omega_m h^2)_{min}$ , where  $(\Omega_m h^2)_{min}$  is the minimum value of  $\Omega_m h^2$  compatible with halo properties, we simply set  $\rho_\chi = \rho_l$  (i.e.,  $\xi = 1$ ). When  $\Omega_\chi h^2 < (\Omega_m h^2)_{min}$ , the neutralino cannot be the unique cold dark matter particle, thus we assign to the neutralino a *rescaled* local density  $\rho_\chi = \rho_l \times \Omega_\chi h^2 / (\Omega_m h^2)_{min}$  (i.e.,  $\xi = \Omega_\chi h^2 / (\Omega_m h^2)_{min}$ )<sup>52</sup>. Thus, summarizing,

$$\rho_\chi = \rho_l, \quad \text{when } \Omega_\chi h^2 \geq (\Omega_m h^2)_{min} \quad (4)$$

$$\rho_\chi = \frac{\Omega_\chi h^2}{(\Omega_m h^2)_{min}} \rho_l, \quad \text{when } \Omega_\chi h^2 < (\Omega_m h^2)_{min}. \quad (5)$$

We stress that in our analyses we consider various scenarios, where neutralinos may constitute the dominant cold dark matter component or only a small fraction of it. As discussed below (see Sect. 4.3), in view of the properties related to detectability of relic neutralinos, it is very important not to disregard neutralino configurations with small relic abundance, where rescaling applies.

#### 4.1.4 Sensitivity range for current WIMP direct searches

In the present paper we focus our analysis to the WIMP mass range which, in the light of the experimental data summarized above and of the previous considerations on the astrophysical uncertainties, appears particularly appealing:

$$40 \text{ GeV} \leq m_W \leq 200 \text{ GeV}. \quad (6)$$

Notice that the mass range of Eq. (6) is quite appropriate for neutralinos. Actually, the lower extreme is indicative of the LEP lower bound on the neutralino mass  $m_\chi$  (in the calculations performed in the present work the actual lower bound



for  $m_\chi$ , dependent on the other susy parameters, is employed, according to the constraints given in <sup>53)</sup>). As for the upper extreme, we notice that, though a generic range for  $m_\chi$  might extend up to about 1 TeV, requirements of no excessive fine-tuning <sup>54)</sup> would actually favour an upper bound of order 200 GeV, in accordance with Eq. (6).

In what follows we will discuss the discovery potential of WIMP direct searches for WIMPs in the mass range of Eq.(6). Particular attention will be paid to capabilities of the present experiments; according to the discussion previously made, their sensitivity range, in case of WIMPs whose coherent interactions with ordinary matter are dominant over the the spin-dependent ones, may be stated, in terms of the quantity  $\xi\sigma_{\text{scalar}}^{(\text{nucleon})}$ , as

$$4 \cdot 10^{-10} \text{ nbarn} \leq \xi\sigma_{\text{scalar}}^{(\text{nucleon})} \leq 2 \cdot 10^{-8} \text{ nbarn.} \quad (7)$$

We will hereafter refer to region  $R$  as the one in the space  $m_W - \xi\sigma_{\text{scalar}}^{(\text{nucleon})}$  which is defined by Eqs. (6-7). The region  $R$  represents the sensitivity region already under exploration with present detectors.

Our analysis, based on an interpretation of experimental data in terms of relic neutralinos, will show by how much the WIMP direct searches probe the supersymmetric parameter space.

## 4.2 WIMP indirect searches

Indirect searches for WIMPs aim at the measurements of signals which fall essentially into two categories (for a review and relevant references see, for instance, Ref. <sup>55)</sup>):

i) Signals due to WIMP pair-annihilations taking place in our galactic halo. The most interesting outputs of these annihilation processes are: a) fluxes of neutrinos and gammas (which might be disentangled from the background in case of halo clumpiness), b) a narrow gamma-gamma line, c) exotic components in cosmic rays: antiprotons, positrons, antideuterons.

ii) Signals due to WIMP pair-annihilations taking place in the interior of celestial bodies. These signals would consist of fluxes of up-going muons in a neutrino telescope, generated by neutrinos which are produced by the pair annihilations of WIMPs captured and accumulated inside the Earth and the Sun.

For the discussion to follow, it is important to notice that in case (i) the detection rates are proportional to  $\rho_W^2 \cdot \sigma_{ann}$ , whereas in case (ii) the detection rates are proportional to  $\rho_W \cdot \sigma_{\text{scalar}}^{(\text{nucleon})}$  (in fact, in this latter case, the annihilation rate

inside the celestial body is proportional to the capture rate of the WIMPs by the body, which is in turn proportional to  $\rho_W \cdot \sigma_{\text{scalar}}^{(\text{nucleon})}$ .

### 4.3 General arguments on detectability of WIMPS versus their local density and average relic abundance

One particular type of relic particle (say, a WIMP) may constitute a dominant or a subdominant dark matter candidate. Also the latter case would be of great physical interest, provided this relic particle has some chance to be detected. Thus, a crucial question is: How do experimental detectabilities of WIMPs depend on the WIMP (local and cosmological) densities ?

This question may be answered by simple general arguments which we already presented in a number of papers (56, 57, 54, 58, 59, 60, 40) and which we briefly review here. Our arguments are exemplified by properties of relic neutralinos, in case these particles decouple from the primordial plasma when in thermodynamic equilibrium. It is obvious that these same arguments apply equally well to other realizations of WIMPs, under the same decoupling conditions.

We consider the rates of direct signals and of signals due to pair annihilation in celestial bodies, separately from the rates of signals due to neutralino–neutralino annihilations taking place in the galactic halo, because of their different dependence on local density and cross sections.

#### 4.3.1 Rates of direct detection and of signals due to pair annihilation in celestial bodies

As was seen above, in both of these experimental measurements the detection rate  $R$  is proportional to the product  $\rho_\chi \cdot \sigma_{\text{scalar}}^{(\text{nucleon})}$ . Thus, taking into account the rescaling properties of  $\rho_\chi$  (Eqs. (4)-(5)), we have that  $R$  behaves as follows

$$R \propto \sigma_{\text{scalar}}^{(\text{nucleon})}, \quad \text{when } \Omega_\chi h^2 \geq (\Omega_m h^2)_{\text{min}} \quad (8)$$

$$R \propto \frac{\Omega_\chi h^2}{(\Omega_m h^2)_{\text{min}}} \sigma_{\text{scalar}}^{(\text{nucleon})} \propto \frac{\sigma_{\text{scalar}}^{(\text{nucleon})}}{\langle \sigma_{\text{ann}} v \rangle}, \quad \text{when } \Omega_\chi h^2 < (\Omega_m h^2)_{\text{min}}. \quad (9)$$

Now, the cross sections  $\sigma_{\text{scalar}}^{(\text{nucleon})}$  and  $\sigma_{\text{ann}}$ , as functions of any generic coupling parameter  $\zeta$ , behave similarly (*i.e.* they usually both decrease or increase in terms of variations of that parameter), because of crossing symmetry. Thus, for instance, in supersymmetric schemes where the neutralino is the LPS,  $\sigma_{\text{scalar}}^{(\text{nucleon})}$  and  $\sigma_{\text{ann}}$  are both increasing functions of  $\tan \beta$ , when the relevant processes are

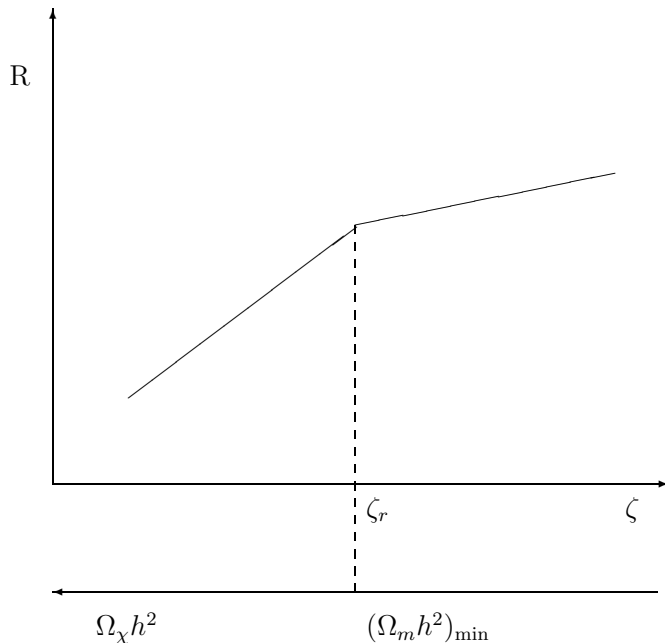


Figure 2: *Qualitative behaviour of the rates of direct detection and of signals due to pair annihilation in celestial bodies as functions of a generic coupling parameter  $\zeta$  ( $\zeta_r$  denotes the value of  $\zeta$  at which  $\Omega_\chi h^2 = (\Omega_m h^2)_{\min}$ ). Notice the correlation between the rates  $R$  and the neutralino relic abundance  $\Omega_\chi h^2$ .*

mediated by Higgs bosons. Usually,  $\sigma_{\text{scalar}}^{(\text{nucleon})}$  increases somewhat faster than  $\sigma_{\text{ann}}$ , or approximately at the same rate. Since, at the same time,  $\Omega_\chi h^2 \propto (\langle \sigma_{\text{ann}} v \rangle)^{-1}$ , the typical behaviour of the rate  $R$  (for the processes under study) is the one displayed in Fig. 2. For small values of  $\zeta$ , both  $\sigma_{\text{scalar}}^{(\text{nucleon})}$  and  $\sigma_{\text{ann}}$  are small (and then  $\Omega_\chi h^2$  is large) and  $R$  grows proportionally to  $\sigma_{\text{scalar}}^{(\text{nucleon})}$ . As the strength of the coupling increases, in the region beyond the value  $\zeta_r$  (at which  $\Omega_\chi h^2 = (\Omega_m h^2)_{\min}$ ), Eq. (9) applies: the rate  $R$  still increases (though less rapidly than before rescaling), or remains approximately flat. Therefore, as far as direct detection and indirect detection through pair annihilation in celestial bodies are concerned, we obtain that *the detectability of relic neutralinos is usually favoured for neutralinos of small  $\Omega_\chi h^2$ , that is for neutralinos which comprise only a subdominant dark matter component.*

We stress that, due to this last property, in the numerical analyses of the properties of relic neutralinos, it is important to keep into consideration also susy configurations where rescaling applies. In fact, by neglecting these configurations, one would disregard relic neutralinos which have the largest chances of being detected. Because of this fact, at variance with most analyses by other authors, our scanning of the susy parameter space always included configurations entailing small

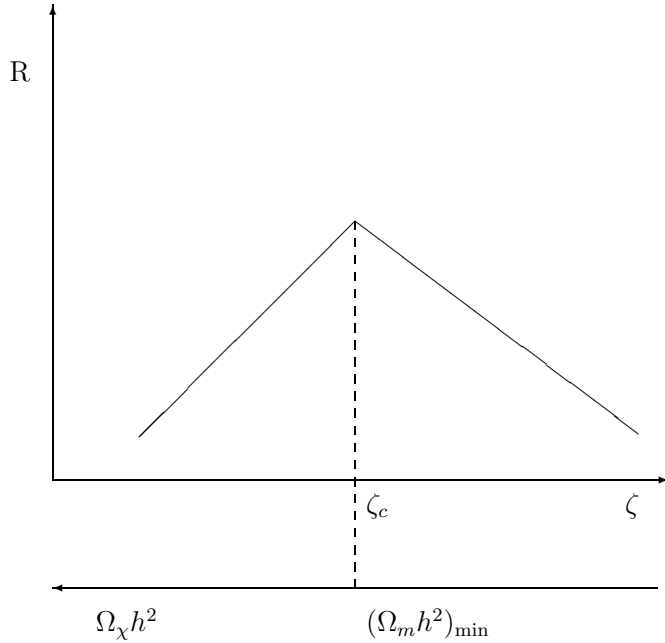


Figure 3: *Qualitative behaviour of the rates of signals due to neutralino–neutralino annihilations taking place in the galactic halo as functions of a generic coupling parameter  $\zeta$  ( $\zeta_r$  denotes the value of  $\zeta$  at which  $\Omega_\chi h^2 = (\Omega_m h^2)_{\min}$ ). Notice the correlation between the rates  $R$  and the neutralino relic abundance  $\Omega_\chi h^2$ .*

neutralino relic abundances (see, for instance, 40)).

The numerical evaluations, which we present in the next section, show that the actual situation is even better; in fact, it turns out that *a number of neutralino configurations of cosmological interest, though disfavoured by the previous arguments, may reach the level of detectability by current experiments.* Actually, we will prove that the annual–modulation effect, measured by the DAMA Collaboration, is compatible with an interpretation in terms of neutralinos, part of which with relic abundance of cosmological interest. Due to the connection between  $\sigma_{\text{scalar}}^{(\text{nucleon})}$  and  $\Omega_\chi h^2$ , this property is far from being trivial.

#### 4.3.2 Rates of signals due to neutralino–neutralino annihilations taking place in the galactic halo.

At variance with the previous case, the detection rates have now a *quadratic* dependence on the neutralino density in the halo,  $R \propto \rho_\chi^2 \cdot \sigma_{\text{ann}}$ ; thus, by using Eqs. (4)-(5), we have the following behaviour for  $R$

$$R \propto \sigma_{ann}, \quad \text{when } \Omega_\chi h^2 \geq (\Omega_m h^2)_{min} \quad (10)$$

$$R \propto \left(\frac{\Omega_\chi h^2}{(\Omega_m h^2)_{min}}\right)^2 \sigma_{ann} \propto \frac{\sigma_{ann}}{\langle \sigma_{ann} v \rangle^2}, \quad \text{when } \Omega_\chi h^2 < (\Omega_m h^2)_{min}. \quad (11)$$

Therefore, in this case, as the generic coupling parameter  $\zeta$  increases, the detection rate first increases, as long as the couplings are small; afterwards, for values of  $\zeta$  larger than  $\zeta_r$ , when rescaling applies, the detection rate decreases (see Fig. 3).

It follows that for processes depending on pair-annihilation in the halo the maximal rates occur for values of the relic abundance around the value  $(\Omega_m h^2)_{min}$ . Subdominant neutralinos are disfavoured for detectability by this type of signals as compared to neutralinos with a relic abundance around the value  $\Omega_\chi h^2 \simeq (\Omega_m h^2)_{min}$ .

Finally, we notice that all the arguments reviewed in this section were already presented in our previous papers (see, for instance, 56, 57, 54), further corroborated by extensive numerical evaluations 58, 59, 60, 40). Amazingly, in a recent preprint 61), where considerations similar to ours are repeated, all previous references have been overlooked.

## 5 Supersymmetric dark matter

We turn now to calculations performed in specific supersymmetric schemes, assuming that R-parity is conserved, and thus that the LSP is stable. The nature of the LSP depends on the susy-breaking mechanism and on the specific regions of the susy parameter space. We consider here gravity-mediated schemes, and domains of the parameter space, where the LSP is the neutralino. Extensive calculations on relic neutralino phenomenology in gravity-mediated models have been performed (see, for instance, Refs. 31–41,49,51–55,57,59–65).

Our analysis will follow the one reported in Ref. 40) and will show by how much the WIMP direct searches probe the supersymmetric parameter space. We remark that, in the case of neutralinos, the assumption about the dominance of the coherent cross section over the spin-dependent one is, in general, largely satisfied, except for values of  $\sigma_{\text{scalar}}^{(\text{nucleon})}$  which are far below the present experimental reach 26).

### 5.1 Susy models

The analysis of Ref. 40) was performed in the Minimal Supersymmetric extension of the Standard Model (MSSM) in a variety of different schemes, from those based on

universal or non-universal supergravity, with susy parameters defined at the grand unification scale, to an effective supersymmetric model defined at the Electro–Weak (EW) scale. Here we only report about results in universal supergravity and in the effective scheme at EW scale; for the other cases and further details we refer to Ref. 40).

The essential elements of the MSSM are described by a Yang–Mills Lagrangian, the superpotential, which contains all the Yukawa interactions between the standard and supersymmetric fields, and by the soft–breaking Lagrangian, which models the breaking of supersymmetry. The Yukawa interactions are described by the parameters  $h$ , which are related to the masses of the standard fermions by the usual expressions, *e.g.*,  $m_t = h^t v_2$ ,  $m_b = h^b v_1$ , where  $v_i$  are the  $vev$ 's of the two Higgs fields,  $H_1$  and  $H_2$ . Implementation of this model within a supergravity scheme leads naturally to a set of unification assumptions at a Grand Unification (GUT) scale,  $M_{GUT}$ :

- i) Unification of the gaugino masses:  $M_i(M_{GUT}) \equiv m_{1/2}$ ,
- ii) Universality of the scalar masses with a common mass denoted by  $m_0$ :  
 $m_i(M_{GUT}) \equiv m_0$ ,
- iii) Universality of the trilinear scalar couplings:  $A^l(M_{GUT}) = A^d(M_{GUT}) = A^u(M_{GUT}) \equiv A_0 m_0$ .

This scheme will be denoted here as universal SUGRA (or simply SUGRA). The relevant parameters of the model at the electro–weak (EW) scale are obtained from their corresponding values at the  $M_{GUT}$  scale by running these down according to the renormalization group equations (RGE). By requiring that the electroweak symmetry breaking is induced radiatively by the soft supersymmetry breaking, one finally reduces the model parameters to five:  $m_{1/2}$ ,  $m_0$ ,  $A_0$ ,  $\tan \beta (\equiv v_2/v_1)$  and sign  $\mu$ . Here the parameters are varied in the following ranges:  $50 \text{ GeV} \leq m_{1/2} \leq 1 \text{ TeV}$ ,  $m_0 \leq 1 \text{ TeV}$ ,  $-3 \leq A_0 \leq +3$ ,  $1 \leq \tan \beta \leq 50$ . Notice that a common upper extreme for the mass parameters has been used, and generically set at the value of 1 TeV, as a typical scale beyond which the main attractive features of supersymmetry fade away. However, fine-tuning arguments actually set different bounds for  $m_0$  and  $m_{1/2}$  (in universal SUGRA and in non–universal SUGRA) <sup>54</sup>):  $m_{1/2} \lesssim$  hundreds of GeV, whereas  $m_0 \lesssim 2 - 3 \text{ TeV}$ . The  $m_0 \sim 2 - 3 \text{ TeV}$  window, which is not specifically included in the results reported here, will be analysed in a forthcoming paper <sup>63</sup>). In Ref. <sup>64</sup>) properties of relic neutralinos in this large  $m_0$  regime have been analyzed. We remark that the phenomenology of relic neutralinos is also very

sensitive to other parameters, such as the top quark mass  $m_t$  and the strong coupling  $\alpha_s$ . For these parameters, we use here their 95% CL ranges:  $m_t = (175 \pm 10)$  GeV and  $\alpha_s(M_Z) = 0.118 \pm 0.004$ .

Models with unification conditions at the GUT scale represent an appealing scenario; however, some of the assumptions listed above, particularly ii) and iii), are not very solid, since, as was already emphasized some time ago <sup>71)</sup>, universality might occur at a scale higher than  $M_{GUT} \sim 10^{16}$  GeV, *e.g.*, at the Planck scale. More recently, the possibility that the initial scale for the RGE running,  $M_I$ , might be smaller than  $M_{GUT} \sim 10^{16}$  has been raised <sup>45, 72)</sup>, on the basis of a number of string models (see for instance the references quoted in <sup>45)</sup>). In Ref. <sup>45)</sup> it is stressed that  $M_I$  might be anywhere between the EW scale and the Planck scale, with significant consequences for the size of the neutralino–nucleon cross section.

An empirical way of taking into account the uncertainty in  $M_I$  consists in allowing deviations in the unification conditions at  $M_{GUT}$ . For instance, deviations from universality in the scalar masses at  $M_{GUT}$ , which split  $M_{H_1}$  from  $M_{H_2}$  may be parametrized as

$$M_{H_i}^2(M_{GUT}) = m_0^2(1 + \delta_i) \quad (12)$$

This is the case of non–universal SUGRA (nuSUGRA) that we considered in Refs. <sup>37, 54, 40)</sup>. Further extensions of deviations from universality in SUGRA models which include squark and/or gaugino masses are discussed, for instance, in <sup>44, 62)</sup>. In this note we do not report results in nuSUGRA schemes; we refer to Ref. <sup>40)</sup> for discussions on this case.

The large uncertainties involved in the choice of the scale  $M_I$  make the SUGRA schemes somewhat problematic: the originally appealing feature of a universal SUGRA with few parameters fails, because of the need to take into consideration the variability of  $M_I$  or, alternatively, to add new parameters which quantify the various deviation effects from universality at the GUT scale. It appears more convenient to work with a phenomenological susy model whose parameters are defined directly at the electroweak scale. We denote here this effective scheme of MSSM by effMSSM. This provides, at the EW scale, a model, defined in terms of a minimum number of parameters: only those necessary to shape the essentials of the theoretical structure of an MSSM, and of its particle content. Once all experimental and theoretical constraints are implemented in this effMSSM model, one may investigate its compatibility with SUGRA schemes at the desired  $M_I$ .

In the effMSSM scheme we consider here, we impose a set of assumptions

at the electroweak scale: a) all trilinear parameters are set to zero except those of the third family, which are unified to a common value  $A$ ; b) all squark soft-mass parameters are taken degenerate:  $m_{\tilde{q}_i} \equiv m_{\tilde{q}}$ ; c) all slepton soft-mass parameters are taken degenerate:  $m_{\tilde{l}_i} \equiv m_{\tilde{l}}$ ; d) the  $U(1)$  and  $SU(2)$  gaugino masses,  $M_1$  and  $M_2$ , are assumed to be linked by the usual relation  $M_1 = (5/3) \tan^2 \theta_W M_2$  (this is the only GUT-induced relation we are using, since gaugino mass unification appears to be better motivated than scalar masses universality). As a consequence, the supersymmetric parameter space consists of seven independent parameters. We choose them to be:  $M_2, \mu, \tan \beta, m_A, m_{\tilde{q}}, m_{\tilde{l}}, A$  and vary these parameters in the following ranges:  $50 \text{ GeV} \leq M_2 \leq 1 \text{ TeV}$ ,  $50 \text{ GeV} \leq |\mu| \leq 1 \text{ TeV}$ ,  $80 \text{ GeV} \leq m_A \leq 1 \text{ TeV}$ ,  $100 \text{ GeV} \leq m_{\tilde{q}}, m_{\tilde{l}} \leq 1 \text{ TeV}$ ,  $-3 \leq A \leq +3$ ,  $1 \leq \tan \beta \leq 50$  ( $m_A$  is the mass of the CP-odd neutral Higgs boson).

The effMSSM scheme proves very manageable for the susy phenomenology at the EW scale; as such, it has been frequently used in the literature in connection with relic neutralinos (often with the further assumption of slepton/squark mass degeneracy:  $m_{\tilde{q}} = m_{\tilde{l}}$ ) [36, 39, 42, 65, 67, 68]. Notice that we are not assuming here slepton/squark mass degeneracy.

We recall that even much larger extensions of the supersymmetric models could be envisaged: for instance, non-unification of the gaugino masses [62, 73], and schemes with CP-violating phases [74]. Here we limit our considerations to the two schemes previously defined: universal SUGRA and effMSSM; for nuSUGRA we refer to Ref. [40].

The neutralino is defined as the lowest-mass linear superposition of photino ( $\tilde{\gamma}$ ), zino ( $\tilde{Z}$ ) and the two higgsino states ( $\tilde{H}_1^0, \tilde{H}_2^0$ ):  $\chi \equiv a_1 \tilde{\gamma} + a_2 \tilde{Z} + a_3 \tilde{H}_1^0 + a_4 \tilde{H}_2^0$ . Hereafter, the nature of the neutralino is classified in terms of a parameter  $P$ , defined as  $P \equiv a_1^2 + a_2^2$ . The neutralino is called a gaugino when  $P > 0.9$ , a higgsino when  $P < 0.1$ , mixed otherwise.

For more details concerning theoretical aspects involved in our calculations we refer to Refs. [37, 39, 40]. Accelerators data on supersymmetric and Higgs boson searches (CERN  $e^+e^-$  collider LEP2 and Collider Detector CDF at Fermilab) provide now rather stringent bounds on supersymmetric parameters. CDF bounds are taken from [75]. The new LEP2 bounds are taken from [53, 76].

As compared to the calculations presented in Ref. [40], we have now implemented effects due to those radiative corrections to the couplings of the neutral Higgs bosons to the quarks which may be sizeable at large  $\tan \beta$  [77]. These radiative corrections affect the calculation of the neutralino-nucleus cross section and of the neutralino cosmological relic abundance. Notice that the correction to the rela-



tion between the  $b$  quark mass and its Yukawa coupling, implied by these radiative corrections, enters also in the calculations of the  $b \rightarrow s + \gamma$  decay (78). For the SUGRA model discussed above, it affects also the boundary conditions at the GUT scale for the  $b$  Yukawa coupling (79). This in turn affects the radiative symmetry breaking mechanism and the low-energy Higgs and sfermion spectra (54). All these effects are included in our calculations.

Finally, we notice that a new experimental constraint on supersymmetric parameters may also be derived from the recent accurate experimental determination of the muon anomalous magnetic moment (8); this measurement provides the value  $a_\mu(\text{exp}) = 11659202(14)(6) \times 10^{-10}$  (1.3 ppm), where  $a_\mu = (g - 2)/2$ . This data, if compared with the theoretical evaluations in Ref. (9), would show a deviation of  $2.6 \sigma$  from the standard-model prediction. This has determined an outburst of theoretical papers (10), where this possible deviation is attributed to supersymmetry, and the relevant implications derived. However, other more recent standard-model evaluations of  $a_\mu$  (11, 12) are in better agreement with the experimental data of Ref. (8) (see also Refs. (13, 14) for detailed discussions of the standard-model calculations of  $a_\mu$ ). Thus, for the time being, it appears safer to use the data of Ref. (8) as a constraint on susy, rather than a sign of it. Employing the theoretical results of Refs. (9, 11, 12), the contribution of supersymmetry to the anomalous moment is constrained by  $-140 \leq a_\mu^{\text{susy}} \cdot 10^{11} \leq 890$ . This constraint has been implemented in our present scanning of the supersymmetric parameter space.

## 5.2 Numerical results

We turn now to the presentation of our results. In Figs. 4-5 we give the scatter plots for  $\sigma_{\text{scalar}}^{(\text{nucleon})}$  versus  $\Omega_\chi h^2$  for two different schemes: universal SUGRA, and effMSSM. For the SUGRA scheme we only display the results corresponding to positive values of  $\mu$ , since, for negative values, the constraint on  $b \rightarrow s + \gamma$  implies a large suppression of  $\sigma_{\text{scalar}}^{(\text{nucleon})}$ . The calculations of  $\sigma_{\text{scalar}}^{(\text{nucleon})}$  have been performed with the formulae reported in Refs. (60); set 1 for the quantities  $m_q < \bar{q}q >$ 's has been used (see Ref. (60) for definitions); the evaluation of  $\Omega_\chi h^2$  follows the procedure given in (66). The two horizontal lines bracket the sensitivity region defined by Eq. (7), when  $\xi$  is set equal to one. The two vertical lines denote the favorite range for  $\Omega_m h^2$ ,  $0.05 \leq \Omega_m h^2 \leq 0.3$ .

Figs. 4-5 provide a first relevant result of our analysis: the present experimental sensitivity in WIMP direct searches allows the exploration of supersymmetric configurations compatible with current accelerator bounds. A number of configura-

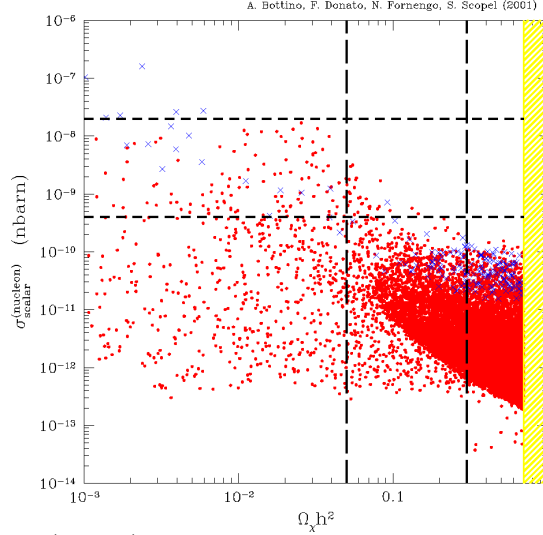


Figure 4: Scatter plot of  $\sigma_{\text{scalar}}^{(\text{nucleon})}$  versus  $\Omega_\chi h^2$  for universal SUGRA. Set 1 for the quantities  $m_q < \bar{q}q >$ 's is employed<sup>60)</sup>. Only configurations with positive  $\mu$  are shown and  $m_\chi$  is taken in the range of Eq. (6). The two horizontal lines bracket the sensitivity region defined by Eq. (7), for  $\xi = 1$ . The two vertical lines denote the range  $0.05 \leq \Omega_m h^2 \leq 0.3$ . The region above  $\Omega_\chi h^2 = 0.7$  is excluded by current limits on the age of the Universe. Dots (crosses) denote gaugino (mixed) configurations.

tions stay inside the region of cosmological interest, also in the constrained SUGRA scheme. The region of experimental sensitivity and cosmological interest is covered with an increasingly larger variety of supersymmetric configurations as one moves from SUGRA to effMSSM; this latter fact is expected from the intrinsic features of the various schemes.

Once a measurement of the quantity  $\rho_\chi \cdot \sigma_{\text{scalar}}^{(\text{nucleon})}$  is performed, values for the local density  $\rho_\chi$  versus the relic abundance  $\Omega_\chi h^2$  may be deduced by proceeding in the following way<sup>60)</sup>:

1)  $\rho_\chi$  is evaluated as  $[\rho_\chi \cdot \sigma_{\text{scalar}}^{(\text{nucleon})}]_{\text{expt}} / \sigma_{\text{scalar}}^{(\text{nucleon})}$ , where  $[\rho_\chi \cdot \sigma_{\text{scalar}}^{(\text{nucleon})}]_{\text{expt}}$  denotes the experimental value, and  $\sigma_{\text{scalar}}^{(\text{nucleon})}$  is calculated as indicated above; 2) to each value of  $\rho_\chi$  one associates the corresponding calculated value of  $\Omega_\chi h^2$ . The scatter plot in Fig. 6 is derived from the lowest value of the annual-modulation region of Ref. <sup>34)</sup>,  $[\rho_\chi / (0.3 \text{ GeV cm}^{-3}) \cdot \sigma_{\text{scalar}}^{(\text{nucleon})}]_{\text{expt}} = 1 \cdot 10^{-9}$  nbarn, and by taking  $m_\chi$  in the range of Eq. (6). This plot, obtained in case of effMSSM, shows that the

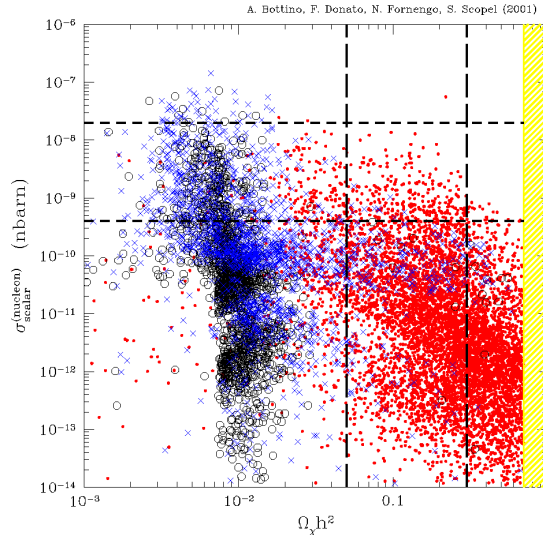


Figure 5: Scatter plot of  $\sigma_{\text{scalar}}^{(\text{nucleon})}$  versus  $\Omega_\chi h^2$  for *effMSSM*. Notations as in Fig. 4. Dots denote gauginos, circles denote higgsinos and crosses denote mixed configurations. Both signs of  $\mu$  are shown.

most interesting region, *i.e.* the one with  $0.2 \text{ GeV cm}^{-3} \leq \rho_\chi \leq 0.7 \text{ GeV cm}^{-3}$  and  $0.05 \leq \Omega_m h^2 \leq 0.3$  (cross-hatched region in the figure), is covered by susy configurations probed by the WIMP direct detection.

Let us examine the various sectors of Fig. 6. Configurations above the upper horizontal line are incompatible with the upper limit on the local density of dark matter in our Galaxy and must be disregarded. Configurations above the upper slanted dot-dashed line and below the upper horizontal solid line would imply a stronger clustering of neutralinos in our halo as compared to their average distribution in the Universe. This situation may be considered unlikely, since in this case neutralinos could fulfill the experimental range for  $\rho_\chi$ , but they would contribute only a small fraction to the cosmological cold dark matter content. For configurations which fall inside the band delimited by the slanted dot-dashed lines and simply-hatched in the figure, the neutralino would provide only a fraction of the cold dark matter at the level of local density and of the average relic abundance, a situation which would be possible, for instance, if the neutralino is not the unique cold dark matter particle component. To neutralinos belonging to these configurations one should assign a *rescaled* local density (see Sect. 4.1.3).

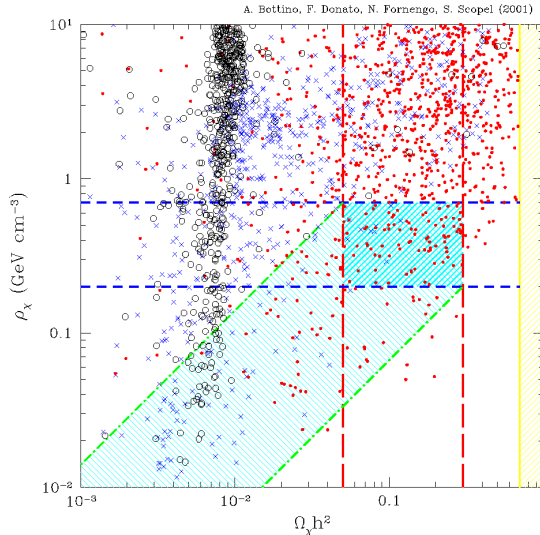


Figure 6: Scatter plot of  $\rho_\chi$  versus  $\Omega_\chi h^2$  for the effMSSM. This plot is derived from the experimental value  $[\rho_\chi / (0.3 \text{ GeV cm}^{-3}) \cdot \sigma_{\text{scalar}}^{(\text{nucleon})}]_{\text{expt}} = 1 \cdot 10^{-9} \text{ nbarn}$  and by taking  $m_\chi$  in the range of Eq. (6), according to the procedure outlined in the text. Set 1 for the quantities  $m_q < \bar{q}q >$ 's is employed<sup>60</sup>). The two horizontal lines delimit the range  $0.2 \text{ GeV cm}^{-3} \leq \rho_\chi \leq 0.7 \text{ GeV cm}^{-3}$ ; the two vertical ones delimit the range  $0.05 \leq \Omega_\chi h^2 \leq 0.3$ . The region above  $\Omega_\chi h^2 = 0.7$  is excluded by current limits on the age of the Universe. The band delimited by the two slanted dot-dashed lines and simply hatched is the region where rescaling of  $\rho_l$  applies. Dots denote gauginos, circles denote higgsinos and crosses denote mixed configurations.

We remind that the scatter plot in Fig. 6 refers to a representative value of  $[\rho_\chi \cdot \sigma_{\text{scalar}}^{(\text{nucleon})}]$  inside the current experimental sensitivity region, thus the plot in Fig. 6 shows that current experiments of WIMP direct detection are probing relic neutralinos which may reach values of cosmological interest, but also neutralinos whose local and cosmological densities may provide only a very small fraction of these densities. These properties were anticipated by the general arguments previously discussed in Sect. IV.C.

For sake of comparison with specific experimental results, we provide in Figs. 7-8 the scatter plots for the quantity  $\xi \sigma_{\text{scalar}}^{(\text{nucleon})}$  versus  $m_\chi$  in the two supersymmetric schemes. In these figures the solid line denotes the frontier of the  $3\sigma$  annual-modulation region of Ref. <sup>34</sup>, when only the uncertainties in  $\rho_l$  and in the dispersion velocity of a Maxwell-Boltzmann distribution, but not the ones in

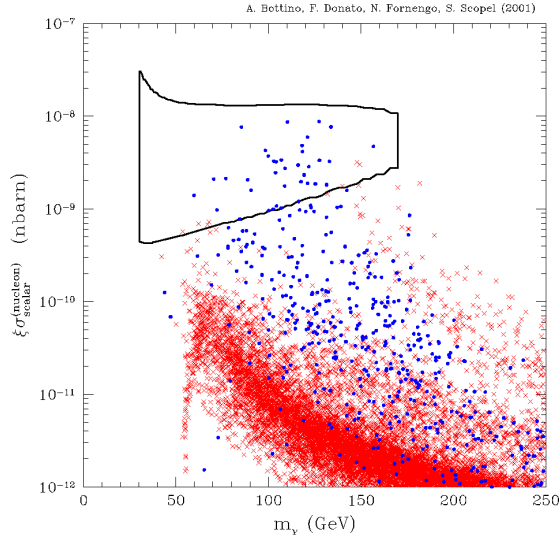


Figure 7: Scatter plot of  $\xi\sigma_{\text{scalar}}^{(\text{nucleon})}$  versus  $m_\chi$  in case of universal SUGRA. Set 1 for the quantities  $m_q < \bar{q}q >$ 's is employed<sup>60</sup>). Crosses (dots) denote configurations with  $\Omega_\chi h^2 > 0.05$  ( $\Omega_\chi h^2 < 0.05$ ). The solid contour denotes the  $3\sigma$  annual-modulation region of Ref.<sup>34</sup>) (with the specifications given in the text).

other astrophysical quantities, are taken into account. As discussed in the Introduction, effects due to a possible bulk rotation of the dark halo or to an asymmetry in the WIMP velocity distribution would move this boundary towards higher values of  $m_\chi$ . Our results in Figs. 7-8 show that the susy scatter plots reach up the annual-modulation region of Ref.<sup>34</sup>), even with the current stringent bounds from accelerators (obviously, more easily in effMSSM than in SUGRA).

Finally, we recall that use of set 2 for the quantities  $m_q < \bar{q}q >$ 's instead of set 1 (see, for definitions, Ref.<sup>60</sup>) would entail an increase of about a factor 3 in all the scatter plots of Figs. 7-8.

## 6 Conclusions

In this work, after a short general introduction, we have shown that the current direct experiments for WIMPs, when interpreted in terms of relic neutralinos, are indeed probing regions of the supersymmetric parameter space compatible with all present bounds from accelerators. We have quantified the extent of the explo-

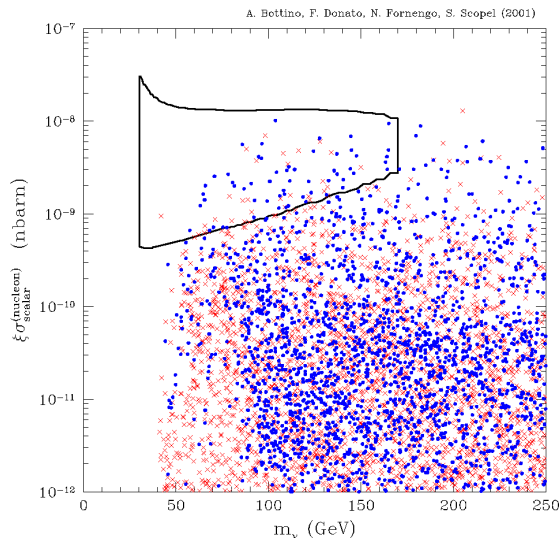


Figure 8: *Same as in Fig. 7 in case of effMSSM.*

ration attainable by WIMP direct experiments in terms of different supersymmetric schemes, from a SUGRA scheme with unification assumptions at the grand unification scale to an effective model, effMSSM, at the electroweak scale. It has been stressed that, due the large uncertainties in the unification assumptions in SUGRA schemes, the effMSSM framework turns out to be the most convenient model for neutralino phenomenology.

We have proved that part of the configurations probed by current WIMP experiments entail relic neutralinos of cosmological interest, and, *a fortiori*, also neutralinos which might contribute only partially to the required amount of dark matter in the Universe. This last property was anticipated by the arguments presented in Sect. 4.3 and confirmed by our numerical results. The cosmological properties have been displayed in terms of a plot of the local density versus the average relic abundance, *i.e.* in a representation which proves particularly useful to summarize the properties of relic neutralinos (see Fig. 6).

The question: *Are relic neutralinos of very low (local and cosmological) densities detectable by current experiments of WIMP direct detection ?* finds a straightforward and affirmative answer in the  $\rho_\chi$  versus  $\Omega_\chi h^2$  plot. *Direct detectability is possible even for neutralino densities quite minuscule as compared to the ones of cosmological interest.*

In the present note, our discussions were mainly focussed on implications of direct detection results. However, as mentioned in Sect. 4.2, also WIMP indirect searches are quite important. Measurements of up-going muon fluxes from the center of the Earth and from the Sun can potentially either find a signal or, at least, place significant constraints (though some uncertainties about a possible solar-bound population have still to be resolved) <sup>39)</sup>. Also measurements of low-energy antiprotons in space may provide interesting constraints on the susy model parameters <sup>39)</sup>, in view of the new refined calculations of secondary antiprotons <sup>80, 81, 82)</sup>.

We notice that, by the arguments presented in Sect. 4.3, similarly to the case of direct detection, the detectability of relic neutralinos by measurements of up-going muon fluxes from the center of the Earth and from the Sun at neutrino telescopes is more favourable in case of low local and average densities.

We have shown that the annual-modulation effect measured by the DAMA Collaboration may be interpreted as due to relic neutralinos, which are compatible with all current constraints from accelerator measurements and WIMP indirect searches.

In our evaluations we have taken into account that the determination of the actual sensitivity region in terms of the WIMP-nucleon cross section and of the WIMP mass from the experimental data depends quite sizeably on uncertainties of various origins, mainly: i) possible effects due to a halo bulk rotation and/or to asymmetries in the WIMP velocities distribution, and ii) significant uncertainties in the determination of Higgs-quark-quark and neutralino-quark-squark couplings. We stress that all these effects have to be taken properly into account, when conclusions about comparison of theory with experiments are drawn.

Finally, we wish to point out that a susy Higgs boson at a mass of about 115 GeV, as possibly hinted by the Higgs LEP experiments <sup>5)</sup>, would fit remarkably well in the scenario depicted above <sup>6)</sup>.

## 7 Acknowledgements

This work was partially supported by the Research Grants of the Italian Ministero dell'Università e della Ricerca Scientifica e Tecnologica (MURST) within the *Astroparticle Physics Project*.

## References

1. See, for instance: J.R. Bond et al., Proc. of IAU Symposium 201 (PASP), CITA-2000-65, astro-ph/0011378; W. Freedman, talk at COSMO2K, Korea, September 2000; W.L. Freedman et al., astro-ph/0012376, ApJ to appear.
2. R.D. Peccei and H. Quinn, Phys. Rev. **D16**, 1791 (1977).
3. H. Murayama, G. Raffelt, C. Hagmann, K. van Bibber and L.J. Rosenberg, Eur.Phys.J. **C15**, 298 (2000).
4. C. Giunti, C.W. Kim and U.W. Lee, Mod. Phys. Lett. **A6**, 1745 (1991); J. Ellis, S. Kelley and D.V. Nanopoulos, Phys. Lett. **B249**, 441 (1990) and Phys. Lett. **B260**, 131 (1991); U. Amaldi, W. de Boer and H. Furstenau, Phys. Lett. **B260**, 447 (1991); P. Langacker and M. Luo, Phys. Rev. **D44**, 817 (1991).
5. Talks given by D. Schlatter (ALEPH Collaboration), T. Camporesi (DELPHI Collaboration), J.J. Blaising (L3 Collaboration), C. Rembser (OPAL Collaboration) at the special seminar at CERN on September 5, 2000 (see links to the LEP experiments at <http://cern.web.cern.ch/CERN/Experiments.html>).
6. A. Bottino, N. Fornengo and S. Scopel, hep-ph/0012377 (to appear in *Nucl. Phys.*).
7. For theoretical considerations about a Higgs boson with a mass of 115 GeV in universal SUGRA see also J. Ellis, G. Ganis, D.V. Nanopoulos and K.A. Olive, Phys. Lett. **B502**, 171 (2001).
8. H.N. Brown et al., Phys. Rev. Lett. **86**, 2227 (2001).
9. M. Davier and A. Höcker, Phys. Lett. **B435**, 427. (1998).
10. A. Czarnecki and W.J. Marciano, hep-ph/0102122; L. Everett, G.L. Kane, S. Rigolin and L.T. Wang, Phys. Rev. Lett. **86**, 3484 (2001); E.A. Baltz and P. Gondolo, Phys. Rev. Lett. **86**, 5004 (2001); U. Chattopadhyay and P. Nath, hep-ph/0102157; S. Komine, T. Moroi and M. Yamaguchi, Phys. Lett. **B506**, 93 (2001) ; R. Arnowitt, B. Dutta, B. Hu and Y. Santoso, Phys.Lett. **B505**, 177 (2001); S.P. Martin and J.D. Wells, hep-ph/0103067; H. Baer, C. Balazs, J. Ferrandis and X. Tata, hep-ph/0103280.
11. S. Narison, hep-ph/0103199.



12. F. Jegerlehner, hep-ph/0104304.
13. W.J. Marciano and B. Lee Roberts, hep-ph/0105056.
14. J.F. de Trocóniz and F.J. Ynduráin, hep-ph/0106025.
15. S. Fukuda et al. (Super-Kamiokande Collaboration), hep-ex/0103033. See also: M.C. Gonzalez-Garcia, M. Maltoni, C. Pea-Garay and J.W.F. Valle, *Phys. Rev. D* **63**, 033005 (2001); G.L. Fogli, E. Lisi, A. Marrone, D. Montanino, A. Palazzo, hep-ph/0104221.
16. T. Toshito (Super-Kamiokande Collaboration), hep-ex/0105023; For a global analysis, which includes all experimental data, see: N. Fornengo, M.C. Gonzalez-Garcia and J.W.F. Valle, *Nucl. Phys. B* **580** 58, (2000).
17. A. Aguilar et al. (LSND Collaboration), hep-ex/0104049.
18. G.F. Giudice, E.W. Kolb and A. Riotto, hep-ph/0005123.
19. V. Berezhinsky, *Nucl. Phys. B (Proc. Suppl.)* **87**, 387 (2000).
20. R. Jeannerot, X. Zhang and R. Brandenberger, *JHEP* **9912**, 003 (1999) ; W. B. Lin, D. H. Huang, X. Zhang and R. Brandenberger, *Phys. Rev. Lett.* **86**, 954 (2001).
21. For a review on WIMP direct searches see, for instance: A. Morales, Proceedings of TAUP99, *Nucl. Phys. B (Proc. Suppl.)* **87**, 477 (2000).
22. A.K. Drukier, K. Freese and D.N. Spergel, *Phys. Rev. D* **33**, 3495 (1986); K. Freese, J. Frieman and A. Gould, *Phys. Rev. D* **37**, 3388 (1988).
23. J. Binney and S. Tremaine, *Galactic Dynamics*, Princeton University Press, Princeton, 1987.
24. E.I. Gates, G. Gyuk and M.S. Turner, *Astrophys. J. Lett.* **449**, L123 (1995).
25. M.W. Goodman and E. Witten, *Phys. Rev. D* **31**, 3059 (1986).
26. A. Bottino, F. Donato, G. Mignola, S. Scopel, P. Belli and A. Incicchitti, *Phys. Lett. B* **402**, 113 (1997).
27. R. H. Helm, *Phys. Rev.* **104**, 1466 (1956).

28. E. Garcia et al., *Phys. Rev.* **D51**, 1458 (1995); A. Morales et al., hep-ex/0101037; L. Baudis et al., *Phys. Rev.* **D59**, 022001 (1999); A. Morales et al., *Phys. Lett.* **B489**, 268 (2000).
29. A. Benoit et al., astro-ph/0106094.
30. R. Bernabei et al., *Phys. Lett.* **B389**, 757 (1996).
31. R. Bernabei et al., *Phys. Lett.* **B436**, 379 (1998).
32. N.J.C. Spooner et al., *Phys. Lett.* **B473**, 330 (2000).
33. R. Bernabei *et al.* (DAMA Collaboration), *Phys. Lett.* **bf B 424**, 195 (1998).
34. R. Bernabei *et al.* (DAMA Collaboration), *Phys. Lett.* **B 480**, 23 (2000); *Eur. Phys. J.* **C 18**, 283 (2000); preprint ROM2/2000-32, to appear in the Proceedings of the PIC20 Conference, <http://www.lngs.infn.it/lngs/htexts/dama/dama7.html>.
35. R. Abusaidi *et al.* (CDMS Collaboration), *Phys. Rev. Lett.* **84**, 5699 (2000).
36. A. Bottino, F. Donato, N. Fornengo and S. Scopel, *Phys. Lett.* **B 423**, 109 (1998); *Phys. Rev.* **D 59**, 095003 (1999).
37. A. Bottino, F. Donato, N. Fornengo and S. Scopel, *Phys. Rev.* **D 59**, 095004 (1999).
38. P. Belli, R. Bernabei, A. Bottino, F. Donato, N. Fornengo, D. Prospero and S. Scopel, *Phys. Rev.* **D 61**, 023512 (2000).
39. A. Bottino, F. Donato, N. Fornengo and S. Scopel, *Phys. Rev.* **D 62**, 056006 (2000).
40. A. Bottino, F. Donato, N. Fornengo and S. Scopel, *Phys. Rev.* **D 63**, 125003 (2001).
41. R. Arnowitt and P. Nath, *Phys. Rev.* **D 60**, 044002 (1999).
42. V.A. Bednyakov and H.V. Klapdor-Kleingrothaus, *Phys. Rev.* **D 62**, 043524 (2000).
43. J. Ellis, A. Ferstl and K.A. Olive, *Phys. Lett.* **B 481**, 304 (2000).

44. E. Accomando, R. Arnowitt, B. Dutta and Y. Santoso, *Nucl.Phys.* **B 585**, 124 (2000).
45. E. Gabrielli, S. Khalil, C. Muñoz and E. Torrente–Lujan, *Phys. Rev.* **D 63**, 025008 (2001).
46. J. Ellis, A. Ferstl and K.A. Olive, *Phys.Rev.* **D63**, 065016 (2001).
47. M. Kamionkowski and A. Kinkhabwala, *Phys. Rev.* **D57**, 3256 (1998) .
48. F. Donato, N. Fornengo and Scopel, *Astrop. Phys.* **9**, 303 (1999).
49. J.D. Vergados, *Phys. Rev.* **83**, 3597 (1998), *Phys. Rev.* **D 62**, 023519 (2000); P. Ullio and M. Kamionkowski, *JHEP* **0103**, 049 (2001).
50. N.W. Evans, C.M. Carollo and P.T. de Zeeuw, astro-ph/0008156.
51. A. M. Green, *Phys.Rev.* **D63**, 043005 (2001).
52. T.K. Gaisser, G. Steigman and S. Tilav, *Phys. Rev.* **D 34**, 2206 (1986).
53. I.M. Fisk and K. Nagai, talks at the XXXth Int. Conf. on High Energy Physics, Osaka, July 2000, <http://www.ichp2000.hep.sci.osaka-u.ac.jp>.
54. V. Berezhinsky, A. Bottino, J. Ellis, N. Fornengo, G. Mignola and S. Scopel, *Astrop. Phys.* **5**, 1 (1996); *Astrop. Phys.* **5**, 333 (1996).
55. A. Bottino and N. Fornengo, Proc. of the Fifth School on Non–Accelerator Particle Astrophysics (Eds. R.A. Carrigan Jr, G. Giacomelli and N. Paver, E.U.T, Trieste, 1999), hep-ph/9904469.
56. A. Bottino, V. de Alfaro, N. Fornengo, G. Mignola and S. Scopel, *Astrop. Phys.* **2**, 77 (1994).
57. A. Bottino, C. Favero, N. Fornengo, G. Mignola and S. Scopel, Proc. of the International Workshop “Double-Beta Decay and Related Topics” (Ed. H.V. Klapdor–Kleingrothaus and S. Stoica, ECT\*/Trento, May–April 1995), 281 (World Scientific, 1996).
58. A. Bottino, C. Favero, N. Fornengo and G. Mignola, *Astrop. Phys.* **3**, 77 (1995).
59. A. Bottino, F. Donato, N. Fornengo and S. Scopel, *Astrop. Phys.* **10**, 203 (1999).
60. A. Bottino, F. Donato, N. Fornengo and S. Scopel, *Astrop. Phys.* **13**, 215 (2000).

61. G. Duda, G. Gelmini and P. Gondolo, hep-ph/0102200.
62. A. Corsetti and P. Nath, hep-ph/0003186.
63. A. Bottino, N. Fornengo and S. Scopel, to be published.
64. J.L. Feng, K.T. Matchev and F. Wilczek, *Phys. Lett* **B482**, 388 (2000).
65. A. Bottino, V. de Alfaro, N. Fornengo, G. Mignola and S. Scopel, *Astrop. Phys.* **1**, 61 (1992).
66. A. Bottino, V. de Alfaro, N. Fornengo, G. Mignola and M. Pignone, *Astrop. Phys.* **2**, 67 (1994).
67. L. Bergström and P. Gondolo, *Astrop. Phys.* **6**, 263 (1996).
68. V. Mandic, A. Pierce, P. Gondolo and H. Murayama, hep-ph/0008022 v2.
69. A.B. Lahanas, D.V. Nanopoulos and V.C. Spanos, hep-ph/0009065.
70. V.A. Bednyakov and H.V. Klapdor–Kleingrothaus, *Phys. Rev.* **D 62**, 043524 (2000); M.E. Gómez and J.D. Vergados, hep-ph/0012020.
71. N. Polonsky and A. Pomarol, *Phys. Rev. Lett.* **73**, 2292 (1994) and *Phys. Rev.* **D 51**, 6532 (1995); M. Olechowski and S. Pokorski, *Phys. Lett.* **B 334**, 201 (1995); D. Metallotakis and H.P. Nilles, *Nucl. Phys.* **B 435**, 115 (1995); A. Pomarol and S. Dimopoulos, *Nucl.Phys.* **B 453**, 83 (1995); H. Murayama, talk given at the 4th International Conference on Physics Beyond the Standard Model, Lake Tahoe, USA, 13–18 december 1994, hep-ph/9503392; J.A. Casas, A. Lleyda and C. Muñoz, *Phys. Lett.* **B 389**, 305 (1996).
72. S.A. Abel, B.C. Allanach, F. Quevedo, L.E. Ibáñez and M. Klein, *JHEP* **0012**, 026 (2000).
73. M. Drees and X. Tata, *Phys. Rev.* **D 43**, 2971 (1991); K. Griest and L. Roszkowski, *Phys. Rev.* **D 46**, 3309 (1992); S. Mizuta, D. Ng and M. Yamaguchi, *Phys. Lett.* **B 300**, 96 (1993).
74. See, for instance: M. Brhlik and G.L. Kane, *Phys. Lett.* **B 437**, 331 (1998); S. Khalil and Q. Shafi, *Nucl. Phys.* **B 564**, 19 (1999); T. Falk, A. Ferstl and K.A. Olive, *Astrop. Phys.* **13**, 301 (2000); P. Gondolo and K. Freese, hep-ph/9908390; S.Y. Choi, hep-ph/9908397.

75. J.A.Valls (CDF Coll.) FERMILAB-Conf-99/263-E CDF;  
<http://fnalpubs.fnal.gov/archive/1999/conf/Conf-99-263-E.html>.
76. P.J. Donan (ALEPH Collaboration), March 2000,  
[http://alephwww.cern.ch/ALPUB/seminar/lepc\\_mar2000/lepc2000.pdf](http://alephwww.cern.ch/ALPUB/seminar/lepc_mar2000/lepc2000.pdf).
77. M. Carena, S. Mrenna and E. E. M. Wagner, *Phys. Rev.* **D60**, 075010 (1999);  
H. Eberl, K. Hidaka, S. Kraml, W. Majerotto and Y. Yamada, *Phys. Rev.* **D62**,  
055006 (2000); A. Djouadi and M. Drees, *Phys. Lett.* **B 484**, 183 (2000).
78. M. Carena, D. Garcia, U. Nierste and C.E.M. Wagner, *Phys. Lett.* **B499**, 141  
(2001); G. Degrassi, P. Gambino and G.F. Giudice, *JHEP* **0012**, 009 (2000).
79. L.J. Hall, R. Rattazzi, U. Sarid, *Phys. Rev.* **D50**, 7048 (1994); R. Rattazzi and  
U. Sarid, *Phys. Rev.* **D53**, 1553 (1996).
80. L Bergström, J. Edsjö and P. Ullio, *Ap.J* **526**, 215 (1999).
81. J.W. Bieber, R.A. Burger, R. Engel, T.K. Gaisser, S. Roesler and T. Stanev,  
*Phys. Rev. Lett.* **83**, 674 (1999).
82. F. Donato, D. Maurin, P. Salati, A. Barreau, G. Boudoul and R. Taillet, *astro-*  
*ph/0103150*.